Earthq Sci (2013) 26(3–4):169–177
DOI 10.1007/s11589-013-0029-9

RESEARCH PAPER

Evaluation of the seismic moment of the April 20, 2013 Lushan earthquake

Xiaogang Hu · Ying Jiang

Received: 25 June 2013 / Accepted: 22 October 2013 / Published online: 20 November 2013

Abstract The April 20, 2013 Lushan earthquake which occurred in Sichuan, China had only moderate thrust. However, the computed seismic moments (M_0) for the Lushan earthquake calculated by several institutions differ significantly from 0.4×10^{19} to 1.69×10^{19} Nm, up to four times difference. We evaluate ten computed M_0s by using normal mode observations from superconducting gravimeters in Mainland China. We compute synthetic normal modes on the basis of moment tensor solutions and fit them to the observed normal modes. Comparison of our results indicates that M_0 is the main cause for some large differences between observations and synthetics. We suggest that a moment magnitude of M_w6.6, corresponding to a M_0 of 0.97–1.08 $\times 10^{19}$ Nm, characterizes the size and strength of the seismic source of the Lushan earthquake.

Keywords Free oscillations · Moment tensor solution · Seismic moment

1 Introduction

A moderate earthquake occurred on April 20, 2013 at Lushan, Sichuan, China. This is in close proximity to the May 12, 2008 Wenchuan earthquake of magnitude M_w7.9. Shortly after the earthquake, several academic institutions including the Chinese Academy of Sciences, the Lamont-Doherty Earth Observatory of Columbia University, and the United States Geological Survey (USGS) reported the moment tensor solutions of the earthquake and concluded that it was a moderate shallow thrust event. Table 1 lists the fault motion parameters and scalar seismic moment (M_0) from ten solutions. The values of M_0 of solutions 8, 9, and 10 are derived from teleseismic inversion rupture processes of the Lushan earthquake. Their results indicated that the source time was about 10 s and rupture size was about 20 km (Wang et al. 2013; Liu et al. 2013a; Zhang et al. 2013). The results in Table 1 show some obvious differences, especially, M_0 differ significantly from 0.4×10^{19} to 1.69×10^{19} Nm, up to 4 times difference, corresponding to moment magnitudes (M_w) varying from 6.37 to 6.8. Such a large discrepancy in the values of predicted M_0 poses the question: which value is the most reliable?

Amplitudes of normal modes are dependent on the location of the epicenter, the seismic station, earthquake depth, focal mechanism, and seismic moment (Stein and Geller 1977). The normal mode is the only seismological signal that can be used to evaluate focal mechanism solutions and constrain the upper limit of the scalar seismic moment of large earthquakes. Observations of oscillatory modes below 1 mHz suggest that the moment magnitude of the 2004 Sumatra megathrust earthquake should be M_w9.3 (Stein and Okal 2005), or M_w9.15 (Park et al. 2005), instead of 9.0 predicted by Global CMT solutions. Note that M_0 of an M_w9.3 earthquake is about 2.5 times larger than the M_0 of an M_w9.0 earthquake. For the great Tohuku earthquake on March 11, 2011, observations of mode$_0$ S_0 suggest that the dip angle provided by the USGS Centroid Moment Tensor Solution might be excessive (Xue et al. 2012). As a typical moderate earthquake, the Lushan event only generated observable signals with spheroidal modes in the range 2.5–5.5 mHz. According to Aki's theory (Aki 1967), normal modes below 5.5 mHz should be sufficient to evaluate the seismic moment M_0 of moderate events.

X. Hu (✉) · Y. Jiang
Laboratory of Geodesy and Earth's Dynamics, Institute of Geodesy and Geophysics, Chinese Academy of Sciences, Wuhan 430077, China
e-mail: hxg432@whigg.ac.cn

Table 1 Ten focal mechanism solutions for the April 20, 2013 Lushan earthquake

Solutions	Strike (deg.)	Dip (deg.)	Slip (deg.)	Depth (km)	M_0 (Nm)	M_W	Data used
1	210	38	96	21.8	1.06×10^{19}	6.6	Far-field body and surface waves
2	198	33	71	10	1.00×10^{19}	6.6	Teleseismic body and surface waves
3	218	39	103	11	0.97×10^{19}	6.6	Far-field W-phase waves
4	216	47	93	19	0.72×10^{19}	6.5	Far-field body waves
5	210	44	91	16	1.09×10^{19}	6.66	Regional and Far-field body waves
6	214	39	100	19	0.40×10^{19}	6.37	Regional body waves
7	216	43	93	12	1.54×10^{19}	6.7	Regional and Far-field body waves
8	205	38.5	88.8	10.2	1.54×10^{19}	6.7	Far-field body waves
9	214	38	91	15	1.01×10^{19}	6.6	Far-field body waves
10	218	39	103	11	1.69×10^{19}	6.8	Far-field body waves

1. Global CMT Project Moment Tensor Solution from the Lamont-Doherty Earth Observatory of Columbia University (http://www.globalcmt.org/)
2. USGS Centroid Moment Tensor Solution (USGS technical report 1)
3. USGS WPhase Moment Tensor Solution (USGS technical report 2)
4. USGS Body-Wave Moment Tensor Solution (USGS technical report 3)
5. Solution from Institute of Geodesy and Geophysics, Chinese Academy of Sciences (Xie et al. 2013)
6. Solution from China Earthquake Networks Center (Liu et al. 2013b)
7. Solution from University of Chinese academy of Sciences (Zhen et al. 2013)
8. Rupture process inversion result (Wang et al. 2013)
9. Rupture process inversion result (Liu et al. 2013a)
10. Rupture process inversion result (Zhang et al. 2013)

This study shows that the M_0 of the Lushan earthquake can be evaluated by normal mode observations made by superconducting gravimeters (SGs) in Mainland China.

2 Methods

Displacement at a seismic station caused by Earth's free oscillations can be modeled using the moment tensor solution of the earthquake and the Green's function, which represents the impulse response of the medium between source and receiver and thus contains the seismic wave propagation effects through the medium from source to receiver. These include energy losses through reflection and transmission at seismic discontinuities, anelastic absorption, and geometrical spreading.

By using a seismic signal that has much longer wavelengths than the dimensions of the source (point source approximation), the observed displacement within seismic source time $\bar{t}$ on the Earth's surface at a station at time t can be expressed as a linear combination of the second-order seismic moment tensor elements convolved with the derivative of the Green's functions (Backus and Mulcahy 1976; Stump and Johnson 1977; Aki and Richards 1980).

$$u_n(\vec{x},t) = [G_{\mathrm{nk},j}(\vec{x},\vec{\xi},t,\bar{t}) * M_{\mathrm{kj}}(\vec{\xi},\bar{t})] \quad (1)$$

where * denotes the temporal convolution, and

$\vec{x}$: position vector of station with coordinates x_1, x_2, x_3 for north, east, and down.

$\vec{\xi}$: position vector of point source with coordinates ξ_1, ξ_2, ξ_3 for north, east, and down.

$u_n(\vec{x},t)$: component of displacement at position $\vec{x}$ and time t. The subscripts $n = 1, 2, 3$ indicate the components for north, east, and down, respectively.

$G_{\mathrm{nk},j}(\vec{x},\vec{\xi},t,\bar{t})$: derivative of Green's function components with regard to source coordinate ξ_j.

$M_{\mathrm{kj}}(\vec{\xi},\bar{t})$: components of the second-order moment tensor released at source time $\bar{t}$.

If all the components of seismic moment tensor have the same time dependence $s(\bar{t})$(synchronous source, Silver and Jordan 1982), the equation (1) can be written as (Stump and Johnson 1977):

$$u_n(\vec{x},t) = [G_{\mathrm{nk},j}(\vec{x},\vec{\xi},t,\bar{t}) * s(\bar{t})]M_{\mathrm{kj}}(\vec{\xi}) \quad (2)$$

If the time function $s(\bar{t})$ is a delta function $\delta(\bar{t})$, the equation (2) can be simplified as (e.g., Jost and Herrmann 1989, Lay and Wallace T 1995; Udías 1999):

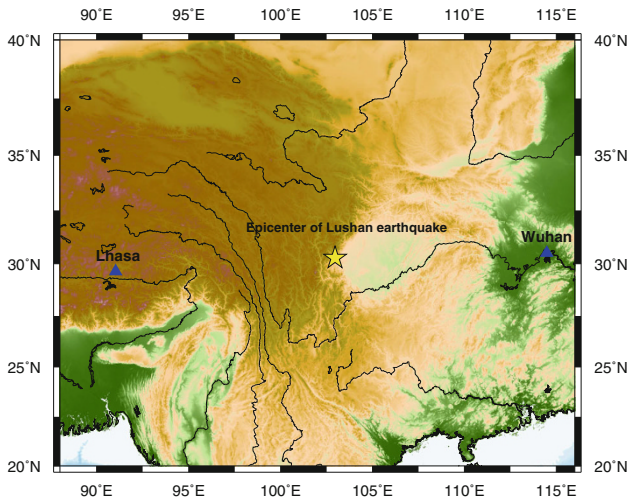

Fig. 1 The locations of Lhasa and Wuhan Stations and the epicenter of the Lushan earthquake on April 20, 2013

$$u_n(\vec{x},t)=\sum_{k=1}^{3}\sum_{j=1}^{3}\frac{\partial G_{\mathrm{nk}}(\vec{x},\vec{\xi},t)}{\partial\xi_j}M_{\mathrm{kj}}(\vec{\xi}) \tag{3}$$

In this case, the nine components of derivative of Green's function describe nine generalized couples. The component with respect to the source coordinate ξ_j is equivalent to a single couple with arm in the ξ_j direction. The Cartesian components of the symmetrical moment tensor in (3) in an isotropic medium for a double couple source can be expressed in terms of strike φ, dip δ, and slip λ of the source and the scalar seismic moment M_0 (Aki and Richards 1980; Jost and Herrmann 1989):

$$\begin{aligned}
M_{11}&=-M_0\left(\sin\delta\cos\lambda\sin2\varphi+\sin2\delta\sin\lambda\sin^2\varphi\right)\\
M_{22}&=M_0\left(\sin\delta\cos\lambda\sin2\varphi-\sin2\delta\sin\lambda\cos^2\varphi\right)\\
M_{33}&=M_0\sin2\delta\sin\lambda\\
M_{12}&=M_0(\sin\delta\cos\lambda\cos2\varphi+0.5\sin2\delta\sin\lambda\sin2\varphi)=M_{21}\\
M_{13}&=-M_0(\cos\delta\cos\lambda\cos\varphi+\cos2\delta\sin\lambda\sin\varphi)=M_{31}\\
M_{23}&=-M_0(\cos\delta\cos\lambda\sin\varphi-\cos2\delta\sin\lambda\cos\varphi)=M_{32}
\end{aligned} \tag{4}$$

The synthetic normal modes can be computed according to focal mechanism solutions, Green's function and equation (3) and (4). As normal modes are very long-period seismic waves, it is sufficient to calculate normal mode displacement caused at a station based on the Green's function derived from 1-D Earth's model, such as PREM (Dziewonski and Anderson 1981). By comparing the synthetic normal modes with the observed modes, we can evaluate focal mechanism solutions in Table 1 for the Lushan earthquake.

Normal modes in 2.5–5.5 mHz were clearly observed by two SGs in Mainland China after the Lushan earthquake. OSG057 and OSG053 are about 1,149 and 1,060 km away from the epicenter, locating at Lhasa and Wuhan stations (see Fig. 1). The seismic source of the Lushan earthquake can be regarded as a point source for observations made at the stations for which the distances to the source are much greater than the linear dimension of the source.

Since SGs have constant scale factor and stable, flat transfer functions in the amplitude and period bands from DC to 100 s, SGs theoretically have an advantage over most broadband seismometers in detailed analyses of the amplitude variations of normal modes and the Earth's hum. In fact, at frequencies below 4 mHz the noise levels of OSG057 and OSG053 are much lower than those of broadband seismometers in Mainland China. For example, normal mode signals cannot be clearly identified in the broadband seismometer STS-2 at Lhasa after the Lushan earthquake.

We calculated theoretical tidal signals for Lhasa and Wuhan Stations and then substracted them from the SG data. We also removed noise signals caused by local air-pressure variations from the data, which may affect the amplitudes of oscillatory modes below 3 mHz (Zürn and Widmer 1995; Hu et al. 2005; Hu et al. 2006). Synthetic normal modes are calculated using the Mineos software package (http://www.geodynamics.org/cig/software/mineos). We perform discrete Fourier transforms on both the corrected data and the synthetic data to get the amplitude spectra.

3 Observations

Figure 2a–c shows ten comparisons among the amplitude spectra at Lhasa. The synthetic spectra, based on solutions 1, 2, 3, 5, and 9 (see Table 1), fits the observations well; however, there are significant differences between the remaining synthetic data and the observations. Table 2 lists these differences between the synthetic data and observations at Lhasa. Synthetic modes derived from solution 6 have the smallest average amplitude, only about 0.37 times the observations. Whereas synthetic modes from solution 10 have the largest average amplitudes, about 1.7 times the observations. The average amplitude of synthetic modes derived from solution 10 is about 5 times larger than that from solution 6. Similar results are observed at Wuhan Station (see Fig. 3a–c).

Both the seismic moment M_0 and the fault motion parameters affect the amplitude of the synthetic data. To distinguish between their respective contributions, we assume that the solutions 6 and 10 in Table 1 have the same $M_0 = 1.0 \times 10^{19}$ Nm but fault motion parameters are kept unchanged, and then calculate their moment tensor components by the formula (4). We recompute synthetic normal modes for solutions 6 and 10 according to the

newly calculated moment tensor components. The results are compared in Fig. 4, showing that the discrepancy between them becomes very small. This indicates that M_0 is the main cause for large discrepancies between synthetic modes and observations. Synthetic modes derived from solutions 1, 2, 3, and 4 in Table 1 fit the observed modes well, suggesting that M_w of 6.6, corresponding to $M_0 = 0.97–1.08 \times 10^{19}$ Nm, characterize the size and strength of the seismic source of the Lushan earthquake.

4 Discussions

Scalar seismic moments quantitatively measure the size and strength of a seismic source based on the final static displacement and the rupture area. It is clear that M_0 is associated with displacement at zero frequency. According to Aki (1967), a simple seismic shear source with linear rupture propagation should have a smooth far-field displacement and velocity spectra. The source spectra can be derived from the station spectra after correction of the effects of geometrical spreading and attenuation. According to the ω^{-2} source model (Aki 1967), the spectral amplitude of displacement at a seismic source increases linearly with its seismic moment for frequencies $f < f_c$ (corner frequency), and the increase with moment is reduced for $f > f_c$. The maximum seismic energy is released around f_c because the peak of the ground-velocity spectrum is at f_c. To evaluate M_0 of a great earthquake of $M_w \geq 9.0$, the frequencies of seismic waves have to be less

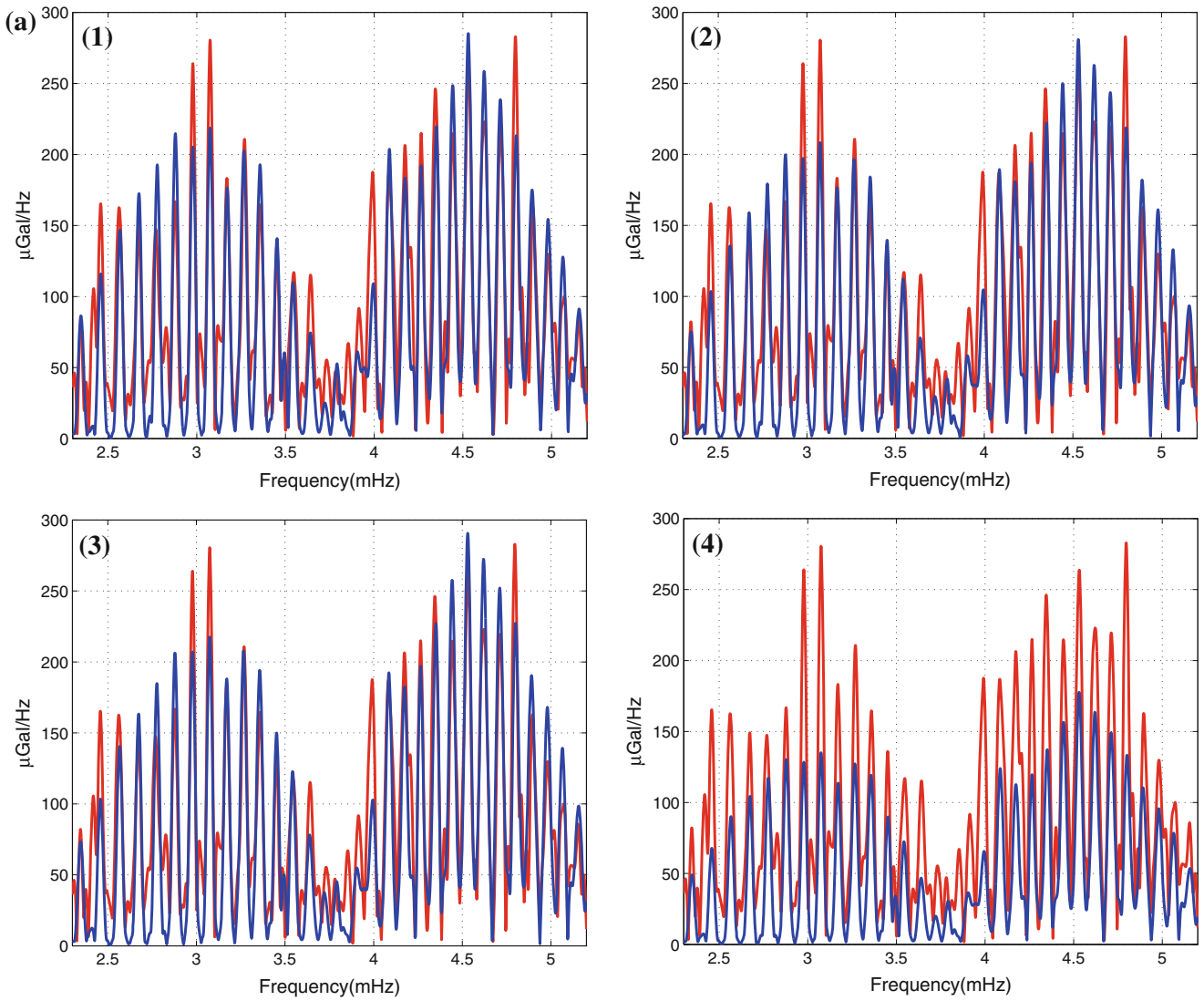

Fig. 2 **a** Comparisons among synthetic modes (*blue*) and SG observations (*red*) at Lhasa after the Lushan earthquake. Numbers 1–10 denote the synthetic modes derived from the solutions listed in Table 1. **b** The same as Fig. 1a, but the synthetic modes are derived from solutions 5–7. **c** The same as Fig. 1a, but the synthetic modes are derived from solutions 8–10

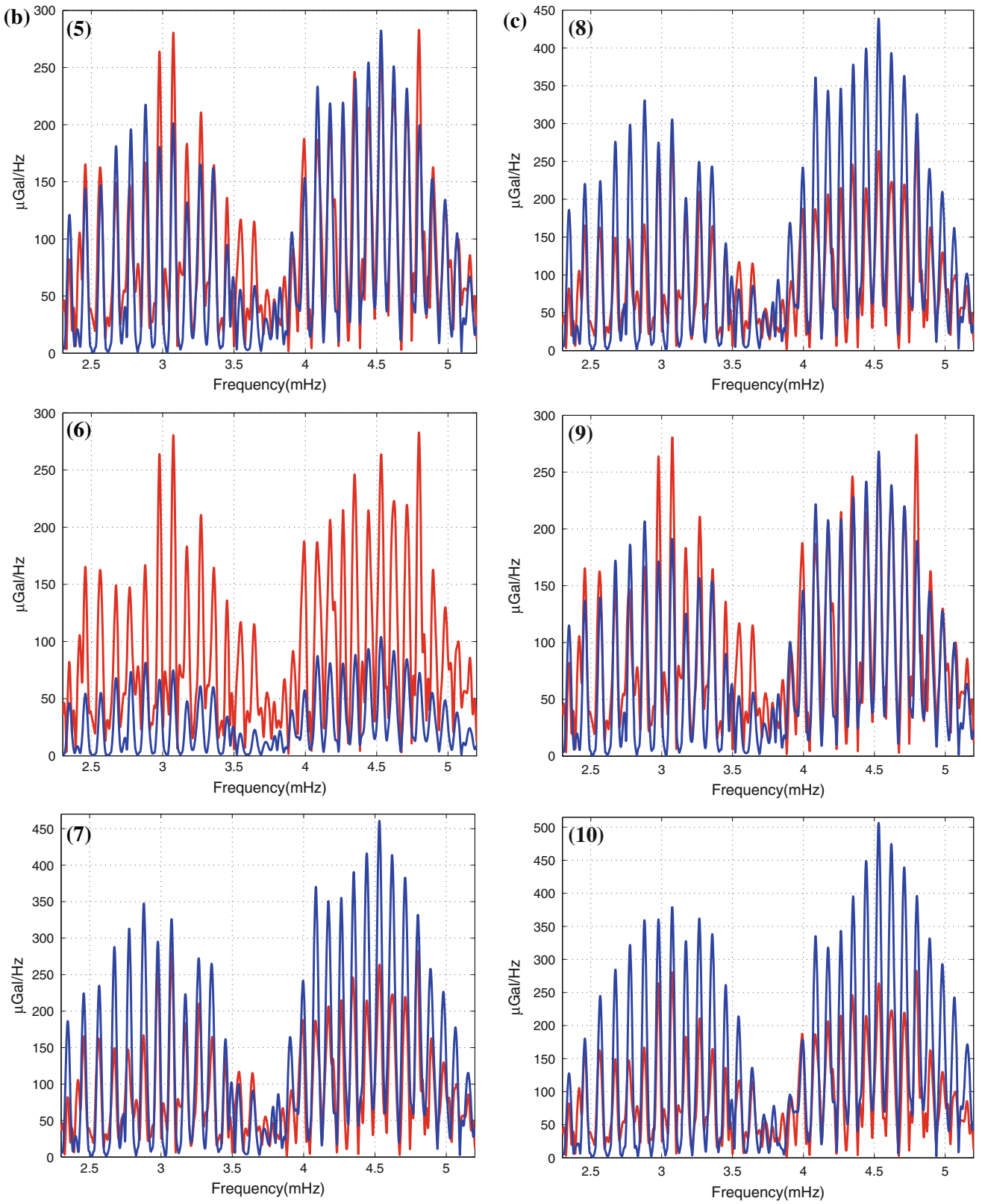

Fig. 2 continued

Table 2 Amplitude differences between synthetic modes and observations at Lhasa

Solutions	1	2	3	4	5	6	7	8	9	10
A/B*	0.9841	0.9520	0.9842	0.6232	1.0058	0.3674	1.5980	1.5179	0.9630	1.7147
Discrepancy (%)	1.59	4.80	1.58	37.68	0.58	63.26	59.80	51.79	3.9	71.47

* A is the average spectral amplitude for synthetic modes in 2.3–5.5 mHz, B is for the observed modes

than 1.0 mHz, but for a moderate earthquake (about M_w 6.5), the frequencies need to be less than 20 mHz. Thus, normal modes within range of 2–5.5 mHz are sufficient to evaluate the seismic moment of the Lushan event.

The USGS Body-Wave Moment Tensor Solution (USGS BMT) according to Sipkin (1982, 1986) uses 15–55 s passband filtered body waveform data. Therefore, this procedure underestimates M_0 for a really great earthquake, mainly because the frequencies of body waveform are much higher than the corner frequency f_c of the great earthquake. The USGS significant earthquake archives used now do not provide the result of USGS BMT for

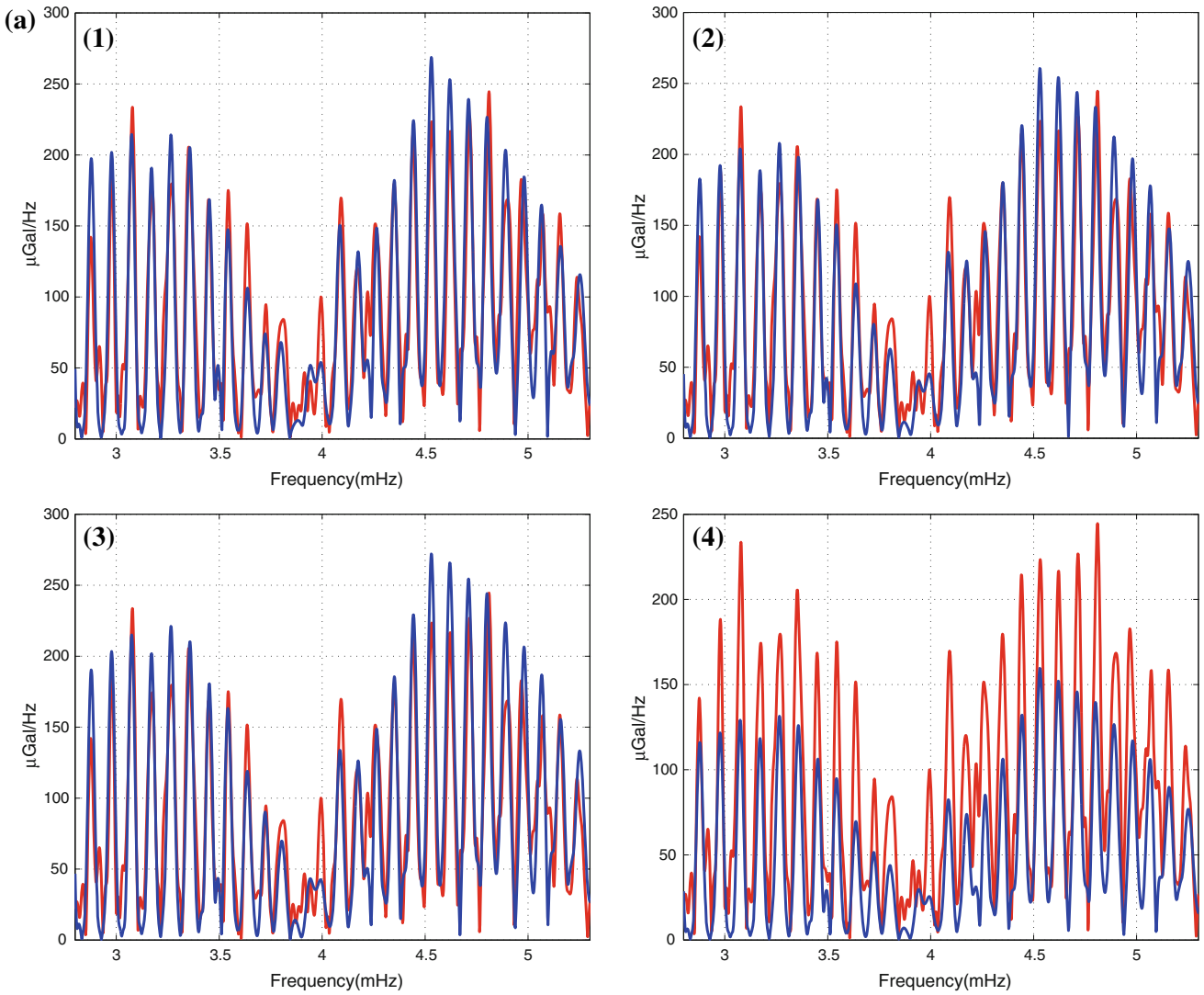

Fig. 3 **a** Comparisons among synthetic modes (*blue*) and SG (*red*) observations at Wuhan after the Lushan earthquake. Numbers 1–10 denote the synthetic modes derived from the solutions listed in Table 1. **b** The same as Fig. 2a, but the synthetic modes are derived from solutions 5–7. **c** The same as Fig. 2a, but the synthetic modes are derived from solutions 8–10

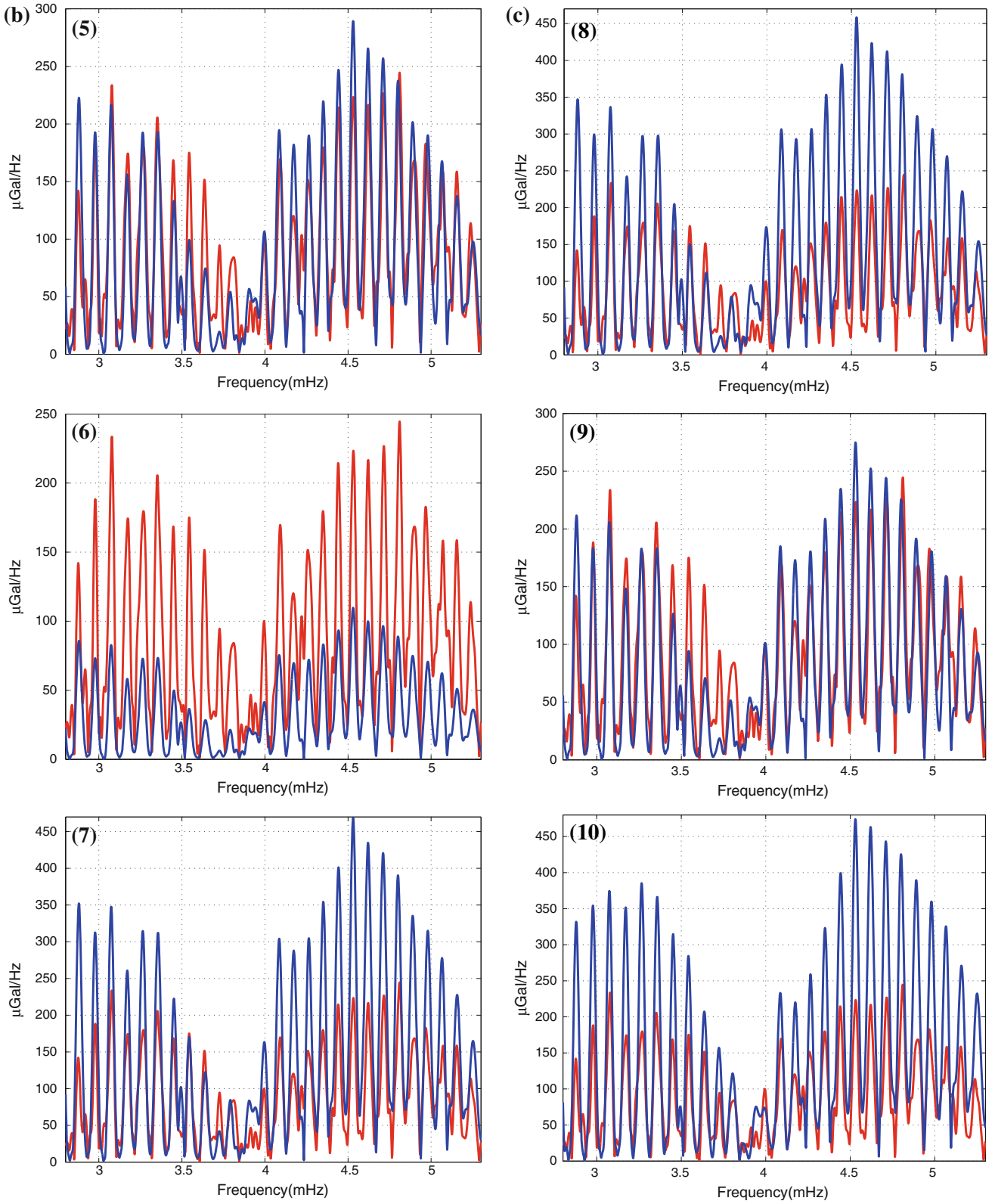

Fig. 3 continued

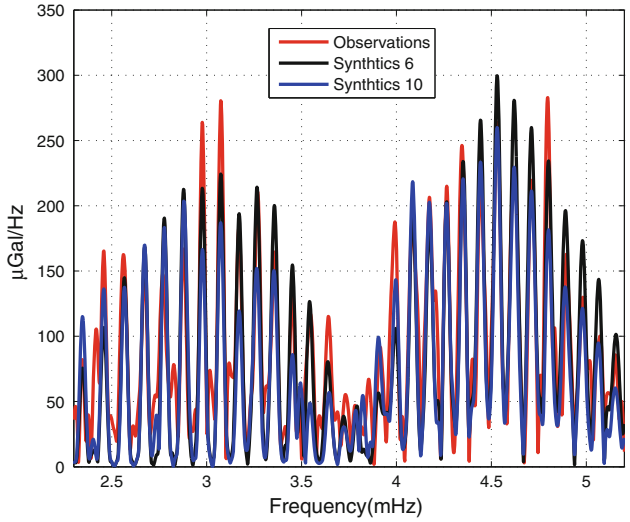

Fig. 4 Comparisons among synthetic modes (*black dash*) and SG (*red*) observations at Lhasa by assuming that synthetic modes have the same seismic moment $M_0 = 1.0 \times 10^{19}$. Synthetics 6 and 10 denote the moment motion parameters provided by the solutions 6 and 10 in Table 1

earthquakes of $M_w > 8.0$. For a moderate earthquake ($5.0 < M_w < 7.0$), the M_0 from USGS BMT usually is slightly less than those from Global CMT Project Moment Tensor Solution (Global CMT). That the M_0 predicted by USGS BMT for the Lushan earthquake is about 70 % less than M_0 by Global CMT presumably reflects slow slip which was not detectable from the body waves.

The synthetic modes derived from the moment tensor solutions 1, 2, 3, and 5 in Table 1 fit the observed modes well in a wide range of 2.5–5.5 mHz, suggesting that synchronous processes played a key role in the rupture propagation of the Lushan event. Solutions 5, 6, and 7 used body wave data and similar inversion methods, CAP or modified CAP method (Zhao and Helmberger 1994; Zhu and Helmberger 1996), but they used different station observations, source time, and velocity model of seismic waves. The predicted M_0s from the three solutions differ significantly. This result confirms that the predicted M_0s not only depends on the inversion methodology itself, but also on the details of in the calculation, including data quality, azimuthal distribution of seismic stations, data preprocessing, velocity model, and waveforms used in the inversion. It needs a reliable way to evaluate the values of the predicted M_0s.

M_0s values of solutions 8, 9, and 10 are estimated according to average slip over rupture area, which are results of inversion for rupture process of the Lushan earthquake based on teleseismic body waves and finite-fault models (e.g., Hartzell and Helmberger 1982; Hartzell and Heaton 1983; Olson and Apsel 1982; Ji et al. 2002). Finite-fault rupture models represent the space–time distribution of slip on a parameterized fault surface (usually setting strike and dip of fault slip). Differential times and amplitudes of seismic waves arriving at stations distributed around the source provide the resolution of slip history. The M_0s values provided by the three solutions are directly cacluated by $M_0 = \mu \cdot A \cdot \overline{D}$, where μ is the average shear modulus of the medium around the fault, A the surface area of the rupture, and $\overline{D}$ the average displacement after the rupture. The normal mode observations suggest that M_0s values are significantly overestimated in solutions 8 and 10.

5 Conclusions

Although measuring moment magnitude of an earthquake has become a routine work, there are sometimes significant discrepancies among the predicted M_0s values from different research institutions. The practice used in this paper suggests that the predicted M_0 for the moderate earthquake like Lushan event can be well constrained by normal mode observations in the frequency range of 2–5 mHz. It would be worthwhile to *employ* this method of M_0 evaluation to the general case of a moderate earthquake.

Acknowledgments This study is supported by National Natural Science Foundation of China (Nos. 41174022 and 41021003).

References

Aki K (1967) Scaling law of seismic spectrum. J Geophys Res 72:1217–1231

Aki K, Richards PG (1980) Quantitative seismology, Freeman, San Francisco, Vol. I and II

Backus G, Mulcahy M (1976) Moment tensors and other phenomenological descriptions of seismic sources-I. continuous displacemenls. Geophys J R Astr Soc 46:341–361

Dziewonski AM, Anderson DL (1981) Preliminary reference Earth model. Phys Earth Planet Inter 25:297–356

Hartzell SH, Heaton TH (1983) Inversion of strong ground motion and teleseismic waveform data for the fault rupture history of the 1979 Imperial Valley, California earthquake. Bull Seismol Soc Am 73:1553–1583

Hartzell SH, Helmberger DV (1982) Strong-motion modeling of the Imperial Valley earthquake of 1979. Bull Seismol Soc Am 72:571–596

Hu XG, Liu LT, Hinderer J, Sun HP (2005) Wavelet filter analysis of local atmospheric pressure effects on gravity variations. J Geod 79:447–459

Hu XG, Liu LT, Hinderer J, Hsu HT, Sun HP (2006) Wavelet filter analysis of atmospheric pressure effects in the long-period seismic mode band. Phys Earth Planet Inter 154:70–84

Ji C, Wald DJ, Helmberger DV (2002) Source description of the 1999 Hector Mine, California, earthquake, part I: wavelet domain inversion theory and resolution analysis. Bull Seismol Soc Am 92:1192–1207

Jost ML, Herrmann RB (1989) A student's guide to and review of moment tensors. Seism Res Lett 60:37–57

Lay T, Wallace TC (1995) Modern global seismology. Academic Press, San Diego. ISBN 0-12-732870-X

Liu CL, Zheng Y, Ge C, Xiong X, Hsu HT (2013a) Rupture Process of the M7.0 Lushan Earthquake. Sci China Earth Sci. doi:10.1007/s11430-013-4639-9

Liu J, Yi GX, Zhang ZW, Guang ZQ, Yuan X, Long F, Du F (2013b) Introduction to Lushan, Sichuan *M*7.0 earthquake on 20 April 2013. Chin J Geophys 56(4):1404–1407. doi:10.6038/cjg201304334 (in Chinese)

Olson AH, Apsel RJ (1982) Finite faults and inverse-theory with applications to the 1979 Imperial Valley earthquake. Bull Seismol Soc Am 72:1969–2001

Park J, Song TRA, Tromp J, Okal E, Stein S, Roult G, Clevede E, Laske G, Kanamori H, Davis P, Berger J, Braitenberg C, Van Camp M, Lei X, Sun H, Xu H, Roast S (2005) Earth's free oscillations excited by the 26 December 2004 Sumatra-Andaman earthquake. Science 308(5725):1139–1144

Silver PG, Jordan TH (1982) Optimal estimation of scalar seismic moment. Geophys J R Astr Soc 70:755–787

Sipkin SA (1982) Estimation of earthquake source parameters by the inversion of waveform data: synthetic waveforms. Phys Earth Planet Inter 30:242–259

Sipkin SA (1986) Estimation of earthquake source parameters by the inversion of waveform data: global seismicity. Bull Seismol Soc Am 76:1515–1541

Stein S, Geller RJ (1977) Amplitudes of the Earth's split normal modes. J Phys Earth 25:117–142

Stein S, Okal EA (2005) Speed and size of the Sumatra earthquake. Nature 308:1127–1139

Stump BW, Johnson LR (1977) The determination of source properties by the linear inversion of seismograms. Bull Seismol Soc Am 67:1489–1502

Udías A (1999) Principles of seismology. Cambridge University Press, United Kingdom

Wang WM, Hao JL, Yao ZX (2013) Preliminary result for rupture process of Apr. 20, 2013, Lushan earthquake, Sichuan, China. Chin J Geophys 56(4):1412–1417. doi:10.6038/cjg201304365 (in Chinese)

Xie ZJ, Jin BK, Zheng Y, Ge C, Xiong X, Xiong C, Hsu HT (2013) Source parameters inversion of the 2013 Lushan earthquake by combining teleseismic waveforms and local seismograms. Sci China Earth Sci. doi:10.1007/s11430-013-4640-3

Xue XX, Hu XG, Hao XG and Liu LT (2012) Constraining focal mechanism of the 2011 Tohoku earthquake by gravity observations. Chin J Geophys 9:3006–3015. doi:10.6038/j.issn.0001-5733.2012.09.019 (in Chinese)

USGS technical report 1 http://earthquake.usgs.gov/earthquakes/eqarchives/fm/neic_b000gcdd_cmt.php. Accessed Nov 2013

USGS technical report 2 http://earthquake.usgs.gov/earthquakes/eqarchives/fm/neic_b000gcdd_wmt.php. Accessed Nov 2013

USGS technical report 3 http://earthquake.usgs.gov/earthquakes/eqarchives/fm/neic_b000gcdd_fmt.php. Accessed Nov 2013

Zhang Y, Xu LS, Chen YT (2013) Rupture process of the Lushan 4.20 earthquake and preliminary analysis on the disaster-causing mechanism. Chin J Geophys 56(4):1408–1411. doi:10.6038/cjg20130435 (in Chinese)

Zhao LS, Helmberger DV (1994) Source estimation from broadband regional seismograms. Bull Seismol Soc Am 84:91–104

Zhen XF, Luo Y, Han LB, Shi YL (2013) The Lushan Ms 7.0 earthquake on 20 April 2013: A High-angle thrust event. Chin J Geophys 56(4):1418–1424. doi:10.6038/cjg20130437 (in Chinese)

Zhu LP, Helmberger DV (1996) Advancement in source estimation techniques using broadband regional seismograms. Bull Seismol Soc Am 86:1634–1641

Zürn W, Widmer R (1995) On noise reduction in vertical seismic records below 2 mHz using local barometric pressure. Geophys Res Lett 22:3537–3540